Vibrational Analysis of Peptides, Polypeptides, and Proteins. XXI. β-Calcium-Poly(L-Glutamate)

PRADEEP K. SENGUPTA and S. KRIMM, *Biophysics Research Division, University of Michigan, Ann Arbor, Michigan 48109*; and S. L. HSU, *Department of Polymer Science and Engineering, University of Massachusetts, Amherst, Massachusetts 01003*

Synopsis

The observed Raman and ir spectra of Ca-poly(L-glutamate) in the β conformation have been analyzed by means of a normal mode calculation. The force field for the main chain was transferred without refinement from β-poly(L-alanine), yet it provides a good prediction of the observed bands and, in particular, explains subtle differences in the spectra of these two β-sheet structures. Main- and side-chain modes are well characterized, and the dependence of the amide III frequency on side-chain composition is again demonstrated.

INTRODUCTION

Ir and Raman spectroscopy, in combination with normal mode analysis, provide a powerful approach for conformational analysis of polypeptides and proteins.[1] Recent efforts in our laboratory have led to the development of refined force fields for polypeptides having α-helix,[2] β-sheet,[3,4] and 3_1-helical[5] conformations. Availability of these force fields has now made it possible to correlate conformational properties with experimentally observed vibrational frequencies with far more confidence and reliability than was heretofore feasible.

Poly(L-glutamic acid) [$(GluH)_n$] offers a particularly interesting case for vibrational analysis of conformation. A great deal of experimental work has been done on $(GluH)_n$, using a wide range of physical techniques, including x-ray and electron diffraction, ir, Raman, and CD. These studies have indicated that under various conditions (depending on temperature, pH, and salt concentration) $(GluH)_n$ can exist as β sheets of different forms, as a random coil, and in α-helix, or so-called "extended helical," conformations.[6-14] Although considerable ir and Raman work has been done on some of these structures by a number of investigators, there are no reports of detailed normal vibrational analyses. Consequently, there has been a limited understanding of the relationship between changes in vibrational spectra and alterations in backbone conformation of the molecule. Furthermore, because of the considerable conformational flexibility inherent in the long side

Biopolymers, Vol. 23, 1565–1594 (1984)

CCC 0006-3525/84/081565-30$04.00

chain of $(GluH)_n$, detailed assignments of the vibrational frequencies are clearly necessary in order to distinguish the conformational changes associated with the side chain from those in the main chain. Only a normal coordinate analysis will permit us to arrive at meaningful conclusions in this regard.

As a first step in this direction, we have examined the β conformation of $(GluH)_n$ in detail. Keith et al. have shown that this polypeptide can be precipitated in the form of small, chain-folded, lamellar single crystals possessing β structure.[8,9] Three distinct modifications of β-$(GluH)_n$ were described by these authors: (a) Crystals of the calcium, strontium, and barium salts, in which the side groups of the polypeptide are ionized and compensated electrostatically by alkaline-earth cations. [These crystals are obtained by slowly heating aqueous solutions containing sodium or ammonium poly(L-glutamate) and a soluble salt (acetate or nitrate) of the corresponding alkaline earth.] (b) Crystals of the free acid obtained from crystals of these alkaline-earth salts by hydrogen-ion exchange in the solid state. (c) Crystals of the free acid precipitated directly from aqueous solutions of the sodium salt by the gradual lowering of the pH.

Itoh et al.[13] obtained two different β forms of $(GluH)_n$, β_I and β_{II}, by heating α-$(GluH)_n$ in the temperature range of 40–85°C and subsequently above 85°C, respectively. Such β_I-$(GluH)_n$ and β_{II}-$(GluH)_n$ appeared to have structural features similar to the β forms prepared by Keith et al.,[8,9] as in (b) and (c) above, respectively. The principal structural features of the different β forms of $(GluH)_n$ have been elucidated by x-ray powder diffraction and selected area electron diffraction analysis.

In the present work, a detailed vibrational analysis of β-Ca-poly(L-glutamate) [β-$(GluCa)_n$] is given. A major factor motivating this initial choice of molecule to study was the availability of atomic coordinates for this compound from the work of Keith et al.[8,9] Secondly, preliminary Raman measurements (Hsu, S.L., unpublished work) on wet crystals of β-$(GluCa)_n$, β-$(GluBa)_n$, and β-$(GluSr)_n$ had indicated that substantially better Raman signals are obtained from the Ca as compared to the other two salts, thus permitting more definitive spectral assignments to be made.

We have carried out a normal mode calculation for the antiparallel-chain pleated-sheet structure of β-$(GluCa)_n$ and its N-deuterated derivative, and have made detailed assignments of observed ir and Raman bands. The good agreement between observed and calculated frequencies serves to confirm the structural proposals for this polypeptide.

MATERIALS AND METHODS

High-molecular-weight samples of $(Glu)_n$ were obtained from New England Nuclear (lot No. G-144, mw $\sim$ 80,000) and Miles Laboratories, Inc. (lot No. GL-133, mw $\sim$ 59,000). Calcium acetate [$Ca(C_2H_3O_2)_2$ ·

H_2O], reagent grade, was obtained from Allied Chemical and used without further purification.

Crystalline β-$(GluCa)_n$ was prepared by following the procedure outlined by Keith et al.[9] The crystals were repeatedly washed with large volumes of deionized water to remove traces of acetate. A partially deuterated sample was prepared by heating the crystals in D_2O at $\sim$ 80°C for over 24 h. In order to obtain more complete deuteration, we prepared a sample by starting with D_2O solutions of Na-poly(L-glutamate) (Sigma Chemical, mw 50,000–100,000) and calcium acetate and using the same protocol as for the NH β crystals. Ir spectra in the amide I (mainly C = O stretch) region confirmed that the samples prepared in this way were indeed in the β conformation.

Raman spectra were obtained by exciting with the 5145 Å line from a SpectraPhysics 165 argon ion laser at a power of 60–110 mW. The scattered light was collected at 90° and analyzed by means of a Spex 1403 double monochromator equipped with a photon-counting detection system. The spectral slit width was 3 cm^{-1}. Collection and processing of the data were handled by a Spex Datamate computer system. All Raman spectra were recorded on samples sealed in glass capillaries. For measurements on wet crystals, slurries of the crystals in H_2O or D_2O were drawn into a capillary and the laser beam was carefully focussed on the solid settled at the bottom.

Ir absorption measurements were made on KBr pellets of samples which had been dried in air or under gentle vacuum, using a concentration of $\sim$ 0.5%. The spectra were recorded on a Digilab FTS-20C FT-ir spectrometer equipped with a HgCdTe detector and purged with dry air. Interferograms (500) were collected at a resolution of 1 cm^{-1}, both for sample and reference (air). The interferograms were separately coadded, Fourier transformed with one level of zero filling, apodized with a triangular function, and the final ratioed spectrum plotted in the transmission mode. A Perkin–Elmer model 180 ir spectrophotometer and a Raman spectrometer described previously[15] were also used for some of the preliminary spectroscopic measurements.

NORMAL MODE CALCULATIONS

Structure, Symmetry, and Selection Rules

Structural information on β-$(GluCa)_n$ was taken from Keith et al.[8] This structure is based on an antiparallel-chain pleated-sheet (APPS) β conformation. The unit cell is monoclinic, having the following dimensions in the wet state: a = 9.40 Å; b = 6.83 Å; c = 12.82 Å; β = 100°20′. The main features of the chain and sheet arrangement are an axial translation per residue of $b/2$ = 3.415 Å, a distance between hydrogen-bonded chains $a/2$ = 4.70 Å, and an intersheet separation of 12.61 Å. From the observed intersheet spacings and electrostatic considerations, Keith et al. concluded that the side chains are fully

extended, with the planes of the carboxylate group essentially parallel to the chain axis (see Fig. 1). Adjacent sheets are displaced by $a/4$ with respect to one another, and are presumably held together by ionic forces. This arrangement gives a fairly open structure, the large spaces between the sheets supposedly being filled, for the wet crystals, by water.

We have taken the structural parameters (bond lengths and bond angles) for the backbone from the x-ray data of Arnott et al. for β-poly(L-alanine)[16] [β-(Ala)$_n$]. We keep the peptide groups strictly planar in order to ensure transferability of force constants. With these conditions, and an axial repeat per residue of 3.415 Å, the dihedral angles are $\phi = -134.84°$, $\psi = 132.01°$. The setting angle α (72.65° in this case), which specifies the orientation of a chain with respect to the sheet, and the side-chain rotation angles, were deduced from the atomic coordinates given by Keith et al.[9] Standard values of bond lengths and bond angles were assumed for the side chain. [This is why the plane of the side-chain atoms departs slightly from being exactly perpendicular to the main-chain axis (cf. Fig. 1).] Furthermore, we have incorporated an axial shift (ΔZ) of -0.27 Å between adjacent hydrogen-bonded chains. As in previous calculations for β-sheet polypeptides,[17] we have relied on amide I band splittings (which arise from transition dipole coupling[18,19]) to calculate the magnitude of the axial shift. Transition dipole coupling energies were calculated for several trial values of ΔZ in the range 0 to $\pm$ 0.4 Å. A value of $\Delta Z = -0.27$ Å gave an optimum fit with the experimentally observed band splittings for amide I. Incidentally, this ΔZ value is identical to that for β-(Ala)$_n$ [cf. the corresponding values of 0 and -0.25 Å for (GlyI)$_n$ and (Ala–Gly)$_n$, respectively[17]]. With the above conditions, the following sheet parameters were deduced: $r(\mathrm{H} \cdots \mathrm{O}) = 1.699$ Å; $r(\mathrm{N} \cdots \mathrm{O}) =$

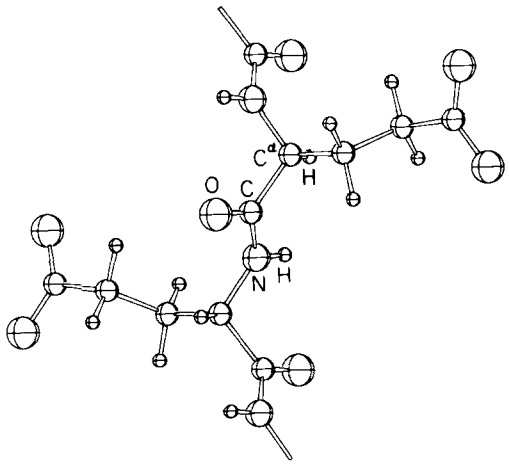

Fig. 1. Single-chain structure of β-Ca-poly(L-glutamate) (Ca^{2+} ions are not shown).

2.694 Å; $r(H^{\alpha} \cdots H^{\alpha}) = 2.151$ Å; $\theta(NH, NO) = 4.20°$; $\gamma(NH \cdots O) = 173.33°$.

The APPS structure belongs to the point group D_2, whose symmetry species show the following activity: $A[\nu(0,0)]$ —R; $B_1[\nu(0,\pi)]$ —R,ir(∥); $B_2[\nu(\pi,0)]$ —R,ir(⊥); $B_3[\nu(\pi,\pi)]$ —R,ir(⊥) (R = Raman). Definitions of the internal and local symmetry coordinates followed our earlier work.[17] The $C^{\delta}O_2$ wagging coordinate was treated as a displacement of the $C^{\gamma}C^{\delta}$ bond from the $C^{\delta}O_2$ plane, and defined by $\Delta\omega = \Delta\alpha_C \sin(OC^{\delta}O)$ (where $\Delta\alpha_C$ is the displacement of the $C^{\gamma}C^{\delta}$ bond with respect to the $OC^{\delta}O$ plane).

Force Field

The force constants for the peptide group as well as the force constants describing the coupling between the C^{β} carbon atom and the peptide backbone, were obtained from the latest β-$(Ala)_n$ force field.[4] In all, 92 nonzero force constants were transferred from β-$(Ala)_n$ and were used without further refinement.

Additional force constants were necessary for the side chain. For the COO^- group, relevant force constants were selectively transferred from work on dipeptides (T. Sundius and S. Krimm, to be published) and tripeptides (A.M. Dwivedi, V. Naik, and S. Krimm, to be published) in the zwitterionic forms. No explicit account was taken of the interaction potential associated with the Ca^{2+} counterions. Force constants for the CH_2—CH_2 group were transferred from *n*-paraffins.[20] Changes were made only in a few cases, when observed ir and Raman data clearly justified such changes. For example, we found it necessary to change $f(C^{\gamma}H)$ from 4.538 to 4.778 and $f(C^{\gamma}H, C^{\gamma}H)$ from 0.019 to 0.064 in order to fit the observed splittings in the Raman frequencies assignable to the $C^{\gamma}H_2$ antisymmetric and symmetric stretch modes. This is not unreasonable, since the presence of the carboxylate group, along with the Ca^{2+} counterions, will presumably affect the electron distribution around neighboring bonds. Therefore, force constants associated with $C^{\gamma}H_2$ stretch frequencies might be expected to differ from corresponding values obtained from purely hydrocarbon force fields. On the same basis, it appeared reasonable to increase the $f(C^{\gamma}C^{\delta})$ force constant slightly, from 4.409 (as obtained from diglycine) to 4.849.

The force constants f(CCH) and f(HCH) and associated interaction force constants were adjusted to reproduce the observed CH_2 bending frequency at 1448 cm^{-1} in the Raman spectrum of the wet crystals. The values finally used for these force constants [f(CCH) = 0.684; f(HCH) = 0.584; f(CCH,CCH) = −0.032; f(CCH,HCH) = 0.037] are, incidentally, very similar to the corresponding force constants for $(GlyI)_n$.[3]

With respect to force constants associated with the COO^- group, $f(C^{\delta}O)$ and $f(C^{\delta}O,C^{\delta}O)$ were altered slightly to fit the observed COO^-

antisymmetric stretch frequency at ~1561 cm^{-1} in the ir, which is a characteristically very strong band. The values which we used are $f(C^5O) = 9.31$ and $f(C^5O,C^6O) = 1.30$, as compared to 9.5 and 1.2, respectively, for the terminal COO^- group of diglycine, from which the force constants were initially transferred. Since the C^6O bond length (1.30 Å), which we took from the x-ray data, is rather high, a lowering of the corresponding stretch force constant would be quite expected, let alone the difference between the carboxylate COO^- group and the terminal peptide COO^- group. The other force constants associated with the COO^- group were used without additional refinement. Table I lists the force constants associated with the side chain.

Transition dipole coupling effects were included for amide I and amide II modes. Effective transition moments of the dipoles, as well as their orientations and locations, were assumed to have the same values as in β-$(Ala)_n$.[17] The range of interaction was ~35 Å within a sheet and ±2 sheets. For amide I the contributions to the various species are: −6(A), 16(B_1), −40(B_2), and 29(B_3) cm^{-1}. For amide II the contributions are: −20(A), −24(B_1), 3(B_2), and 32(B_3) cm^{-1}.

RESULTS AND DISCUSSION

Raman and ir spectra of wet and dry β-$(GluCa)_n$ crystals, respectively, are shown in Figs. 2–5, with their N-deuterated counterparts being given in Figs. 6–8. The observed frequencies, including Raman bands of dry samples, are listed in Tables II and III, together with the calculated frequencies and potential energy distributions (PED).

The NH stretch modes can be assigned to observed Raman bands at 3276 cm^{-1} (wet crystals) and 3274 cm^{-1} (dry crystals), and observed ir bands at 3275 (amide A,ν_A) and 3088 (amide B,ν_B) cm^{-1}. [In most cases, Raman bands are assigned to A species modes, although, of course, contributions from other species cannot at this time be excluded. Since polarization data are not presently available, we assign the ir bands to B_1, B_2, or B_3 species primarily on the basis of the strongest transition-moment direction and by analogy with the results on β-$(Ala)_n$.[4]] Fermi resonance analysis of the observed amide A and B modes[21] gives the unperturbed NH stretch frequency, ν_A^0, at 3230 cm^{-1}. The lower value as compared to that in β-$(Ala)_n$,[4] viz. 3242 cm^{-1}, is consistent with the stronger hydrogen bond in the present case: $r(N \cdots O) = 2.694$ Å as compared to $r(N \cdots O) = 2.731$ Å in β-$(Ala)_n$. Although this would justify a somewhat lower value for the f(NH) force constant, and a slightly higher value of $f(H \cdots O)$, we have not made these small changes at the present time, adhering to a strict transfer of the β-$(Ala)_n$ force field. From this analysis we also find $\nu_B^0 = 3133$ cm^{-1}.

The ND stretch modes are found at ~2463 and 2413 cm^{-1}. As in β-$(Ala\text{–}ND)_n$,[22] the stronger ν_A mode is at the lower frequency. However, there is only one weaker Fermi resonance component in this case in distinction to the two present in β-$(Ala\text{–}ND)_n$.[22] A Fermi resonance

TABLE I
Force Constants for the Side Chain

Force Constant[a]	Value[b]
$f(C^{\alpha}C^{\beta}) = f(C^{\beta}C^{\gamma})^{*}$[c]	4.532
$f(C^{\beta}H^{\beta})^{*}$	4.538
$f(C^{\beta}H^{\beta}, C^{\beta}H^{\beta})^{*}$	0.019
$f(C^{\gamma}H^{\gamma})$	4.778
$f(C^{\gamma}H^{\gamma}, C^{\gamma}H^{\gamma})$	0.064
f(CCH)	0.684
f(HCH)	0.584
f(CCH,CCH)[d]	−0.032
f(CCH,HCH)	0.037
f(CC,CCH)	0.174
f(CCC)*	1.032
f(CC,CC)*	0.083
f(CC,CCH)*	−0.097
f(CC,CCC)*	0.303
f(CCH,CCH)*	0.021
f(CCC,CCH)*	−0.022
$f(\mathrm{CCH,CCH})^{*}_{T}$	0.073
$f(\mathrm{CCH,CCH})^{*}_{G}$	−0.058
$f(\mathrm{CCH,CCH})^{*}_{T}$	−0.009
$f(\mathrm{CCH,CCH})^{*}_{G}$	−0.004
f(CCH,CCH)*	0.012
$f(\mathrm{CCC,CCH})^{*}_{G}$	−0.064
f(CCC,CCC)*	0.097
f(CC t)[e]	0.072
$f(C^{\gamma}C^{\delta}O)$	1.109
$f(OC^{\delta}O)$	2.033
$f(CO_2\ w)$	0.542
$f(C^{\gamma}C^{\delta}\ t)$	0.155
$f(C^{\gamma}C^{\delta})$	4.849
$f(C^{\delta}O)$	9.310
$f(C^{\delta}O,C^{\delta}O)$	1.300
$f(C^{\gamma}C^{\delta},C^{\delta}O)$	1.439
$f(C^{\gamma}C^{\delta},OC^{\delta}O)$	−0.652
$f(C^{\delta}O,C^{\gamma}C^{\delta}O)$	0.509
$f(C^{\delta}O,C^{\gamma}C^{\delta}O')$	−0.509
$f(C^{\delta}O,OC^{\delta}O')$	−0.135
$f(C^{\gamma}C^{\delta}O,C^{\gamma}C^{\delta}O')$	−0.100

[a] f(AB) = AB bond stretch, f(ABC) = ABC angle bend, $f(X,Y)$ = XY interaction, T = *trans*, G = *gauche*, t = torsion, w = wag.

[b] Units are mdyn/Å for stretch and stretch, stretch force constants, mdyn for stretch, bend force constants, and mdyn Å for all others.

[c] An asterisk denotes force constants taken from Snyder (Ref. 22) with no change.

[d] In the nondiagonal force constants, atoms common to the interaction coordinate pair are shown by underlining.

[e] f(CC t), which is given as 0.024 by Snyder, had to be multiplied by three to make it compatible with our definition of the torsional coordinate.

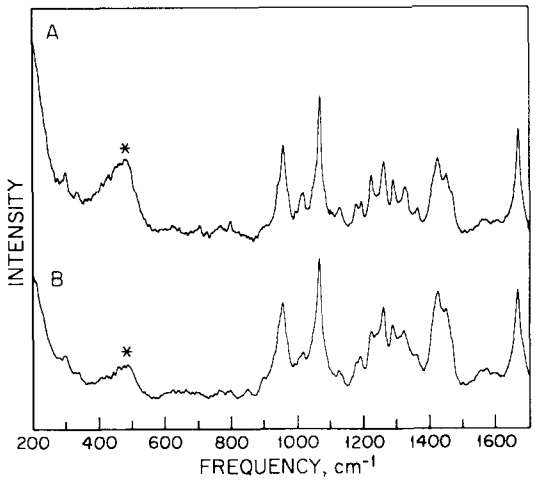

Fig. 2. Raman spectra of β-(GluCa)$_n$ in the 200–1700-cm^{-1} region: (A) wet crystals; (B) dry crystals. (Asterisks denote peaks attributed to glass capillary.)

analysis gives $\nu_A^0 = 2421$ cm^{-1}, which is 7 cm^{-1} below the value for β-(Ala–ND)$_n$,[22] consistent with the stronger hydrogen bond in the present case. From the analysis we also find $\nu_B^0 = 2456$ cm^{-1}. If we assume that the same general kind of combination applies here as in (GlyI–ND)$_n$ and β-(Ala–ND)$_n$,[22] namely, between amide II′ (CN plus C$^\alpha$C stretch) and ND in-plane bend, then (as seen below) the approximate ND in-plane bend mode, observed in the Raman at 992 cm^{-1}, implies that an amide-II′ mode should be found near 2456–992 = 1464 cm^{-1}.

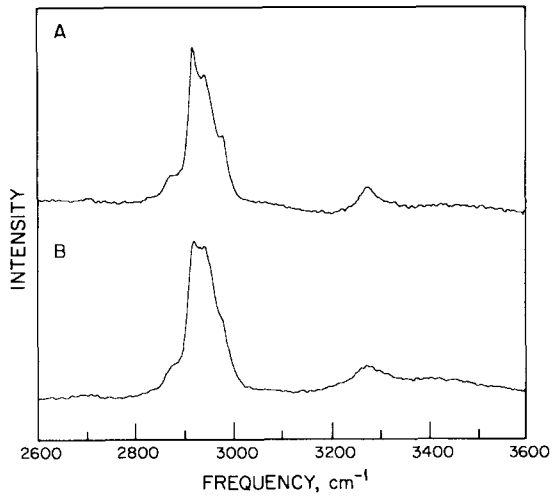

Fig. 3. Raman spectra of β-(GluCa)$_n$ in the 2600–3600-cm^{-1} region: (A) wet crystals; (B) dry crystals. (In the spectrum of the wet crystals, the strong bands due to OH stretch vibrations of H_2O have been removed by computer subtraction.)

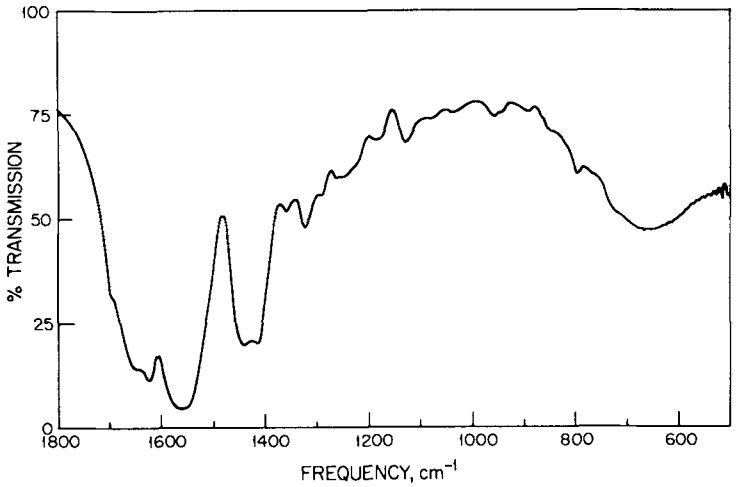

Fig. 4. Fourier-transform ir absorption spectrum of β-(GluCa)$_n$ in the 500–1800-cm^{-1} region.

In fact, we find a new Raman band at 1459 cm^{-1} in β-(GluCa–ND)$_n$ which can be assigned to amide II′ (see below). The species is also appropriate for Fermi resonance interaction with the B_2 ND stretch mode: 1459(A) + 992 (B_2) = 2451(B_2). The ND stretch region thus provides important information on the assignment of lower-frequency modes.

In the CH_2 stretching region, five modes are predicted, and observed Raman bands at 2980, 2942, 2919, and 2877 cm^{-1} in the wet crystals can easily be assigned to four of these. Only three of these modes are seen in the ir. In the Raman spectra of the dried crystals, the above

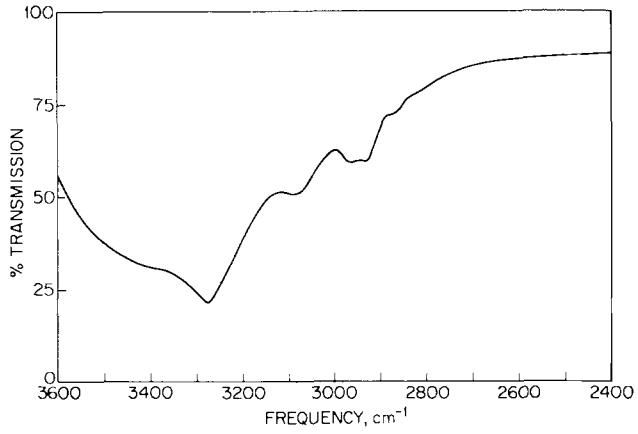

Fig. 5. Fourier-transform ir absorption spectrum of β-(GluCa)$_n$ in NH and CH_2 stretching regions.

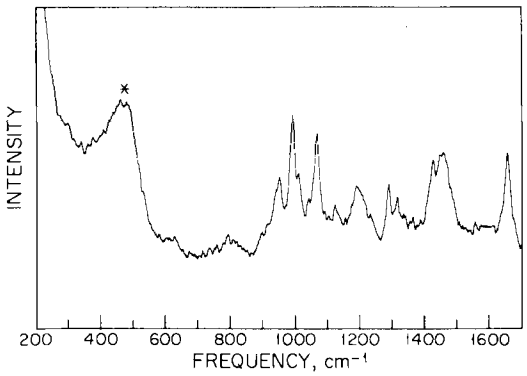

Fig. 6. Raman spectrum of the N-deuterated derivative of β-(GluCa)$_n$ in the 200–1700-cm^{-1} region: wet crystals. (Asterisk denotes peak attributed to glass capillary; the band at 1202 cm^{-1} is due to D_2O.)

four bands are somewhat broadened and less distinct. This may be due to some disorder in the side chains, but since the four bands are still evident, we assume that most of the side chains are in an extended conformation, and therefore in particular the ir spectra (of dried crystals) can be taken as representative of our assumed structure.

The amide I modes are fairly well predicted by our calculations, which give assignments analogous to those for β-(Ala).[4] In addition to KBr pellets, we have recorded the ir spectrum in Nujol mull and as a film of crystals deposited on a AgBr plate. In all these spectra the amide I region showed the same general features, particularly having the very strong ir peak at ~1624 cm^{-1} (in agreement with the results of Keith et al.[9]), thus confirming the presence of the APPS structure

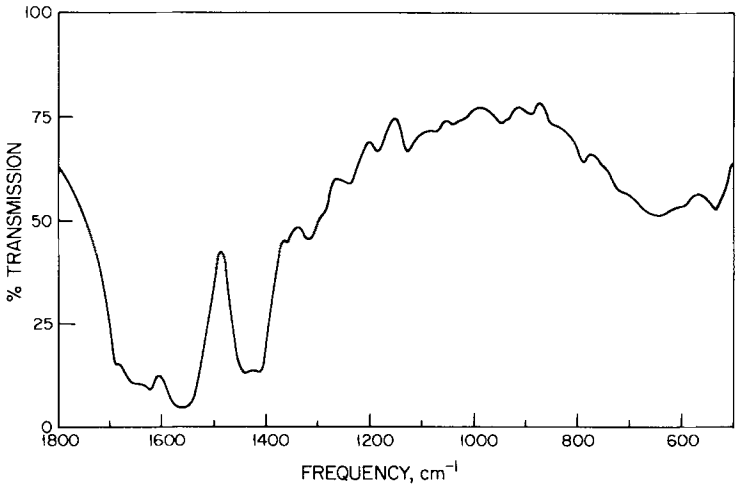

Fig. 7. Fourier-transform ir absorption spectrum of the N-deuterated derivative of β-(GluCa)$_n$ in the 500–1800-cm^{-1} region.

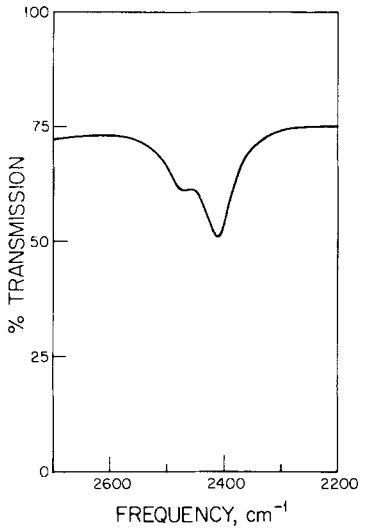

Fig. 8. Fourier-transform ir absorption spectrum of the N-deuterated derivative of β-(GluCa)$_n$ in ND stretching region.

even in the dried crystals. The broad absorption that we find in the 1650–1660 cm^{-1} region indicates the presence of some unordered material, which may result from the drying process or possibly from β-turn structures[23] on the crystal surfaces that result from chain folding.[9] The observed Raman band at 1666 cm^{-1} falls at the lower limit reported for β-sheet conformations.[24] The stronger hydrogen bond in β-(GluCa)$_n$ would be expected to lead to a lower amide I frequency, and this probably also accounts for the lower-frequency ir band (1624 cm^{-1}) as compared to β-(Ala)$_n$ (1632 cm^{-1}).[4] The slight downward shift in amide I frequencies on N-deuteration[4] is also well predicted.

The assignment of the amide II mode (NH in-plane bend plus CN stretch) is particularly difficult for β-(GluCa)$_n$ because the ir spectrum, in which amide II is strongest, is overlapped in this region by the strong COO$^-$ antisymmetric stretch mode at 1561 cm^{-1}. A difference spectrum, normalized to the 1414 cm^{-1} COO$^-$ symmetric stretch mode (and cancelling out, as expected, the CH_2-bend mode at 1440 cm^{-1}) shows a residual band of medium intensity at ~1560 cm^{-1} (see Fig. 9). On the one hand, this would be in reasonable agreement with the appropriate B_1-species mode calculated at 1550 cm^{-1} (although of course this value is obtained from a completely transferred and unrefined force field); its somewhat high value would be unusual but not unknown (cf. 1554 cm^{-1} for this mode in β_2-(GluH)$_n$).[13] On the other hand, this would suggest that the combination responsible for ν_B^0 is A + B_2 (1552 + 1576 = 3128), as may be the case in β-(Ala)$_n$[24]; a B_1 + B_3 combination would require a B_1 amide II mode near the more typical value of 1525 cm^{-1} (where a shoulder is seen in the difference spectrum,

TABLE II
Observed and Calculated Frequencies (cm^{-1}) of β-$(GluCa)_n$

Observed[a]			Calculated				
Wet	Dry						
Raman	Raman	ir	A	B_1	B_2	B_3	Potential Energy Distribution[b]
3276 W[c]	3274 W[c],br		3244				NH s(97)
				3244			NH s(97)
		3230 M[d]			3244		NH s(97)
						3244	NH s(97)
2980 W	2980 sh		2982				$C^{\gamma}H_2$ as(99)
		2965 W,br		2982			$C^{\gamma}H_2$ as(99)
					2982		$C^{\gamma}H_2$ as(99)
						2982	$C^{\gamma}H_2$ as(99)
2942 S	2943 S		2943				$C^{\gamma}H_2$ ss(99)
				2943			$C^{\gamma}H_2$ ss(99)
					2943		$C^{\gamma}H_2$ ss(99)
		2936 W,br				2943	$C^{\gamma}H_2$ ss(99)
2919 VS	2920 S		2918				$C^{\beta}H_2$ as(99)
				2918			$C^{\beta}H_2$ as(99)
					2918		$C^{\beta}H_2$ as(99)
						2918	$C^{\beta}H_2$ as(99)
2877 W	2874 W		2877				$C^{\alpha}H^{\alpha}$ s(96)
						2877	$C^{\alpha}H^{\alpha}$ s(96)
				2867			$C^{\alpha}H^{\alpha}$ s(93)
		2875 W,br			2867		$C^{\alpha}H^{\alpha}$ s(93)
			2855				$C^{\beta}H_2$ ss(97)
				2855			$C^{\beta}H_2$ ss(93)
					2855		$C^{\beta}H_2$ ss(93)
						2855	$C^{\beta}H_2$ ss(97)
						1701	CO s(75), CN s(17)

		1693 sh		1692	CO s(72), CN s(21)
1666 S	1665 S		1668		CO s(73), CN s(20)
		1624 VS		1630	CO s(75), CN s(16)
1598 VW	1595 VW			1607	NH ib(50), CN s(18), $C^{\alpha}C$ s(11)
1567 VW	1569 W			1576	NH ib(50), CN s(19), $C^{\alpha}C$ s(11)
1557 VW	1556 W		1561		$C^{\delta}O_2$ as(87)
		1561 VS		1561	$C^{\delta}O_2$ as(87)
				1561	$C^{\delta}O_2$ as(87)
				1561	$C^{\delta}O_2$ as(87)
			1552		NH ib(58), CN s(19)
		1560 M		1550	NH ib(58), CN s(18)
1462 sh			1461		$C^{\beta}H_2$ b(60), $C^{\gamma}H_2$ b(30)
				1461	$C^{\beta}H_2$ b(60), $C^{\gamma}H_2$ b(30)
				1460	$C^{\beta}H_2$ b(59), $C^{\gamma}H_2$ b(35)
		1452 sh[e]	}	1460	$C^{\beta}H_2$ b(59), $C^{\gamma}H_2$ b(35)
1448 M	1449 M		1448		$C^{\gamma}H_2$ b(64), $C^{\beta}H_2$ b(19)
				1448	$C^{\gamma}H_2$ b(64), $C^{\beta}H_2$ b(19)
				1447	$C^{\gamma}H_2$ b(59), $C^{\gamma}H_2$ b(27)
		1440 S	}	1447	$C^{\gamma}H_2$ b(59), $C^{\beta}H_2$ b(27)
1422 MS	1424 MS		1416		$C^{\delta}O_2$ ss(60), $C^{\delta}O_2$ b(22), $C^{\gamma}C^{\delta}$ s(14)
				1416	$C^{\delta}O_2$ ss(60), $C^{\delta}O_2$ b(22), $C^{\gamma}C^{\delta}$ s(14)
				1416	$C^{\delta}O_2$ ss(58), $C^{\delta}O_2$ b(21), $C^{\gamma}C^{\delta}$ s(13)
		1414 S		1416	$C^{\delta}O_2$ ss(58), $C^{\delta}O_2$ b(21), $C^{\gamma}C^{\delta}$ s(13)
1411 W sh			1414		H^{α} b2(29), $C^{\alpha}C$ s(18), $C^{\beta}H_2$ b(12), $C^{\beta}H_2$ w(11)
				1414	H^{α} b2(29), $C^{\alpha}C$ s(18), $C^{\beta}H_2$ b(11), $C^{\beta}H_2$ w(11)
				1384	$C^{\beta}H_2$ w(44), $C^{\beta}C^{\gamma}$ s(15), H^{α} b1(12), $C^{\alpha}C^{\beta}$ s(10)
				1384	$C^{\beta}H_2$ w(44), $C^{\beta}C^{\gamma}$ s(15), H^{α} b1(12), $C^{\alpha}C^{\beta}$ s(10)
1360 W	1359 W		1368		$C^{\beta}H_2$ w(38), $C^{\gamma}H_2$ w(17), $C^{\beta}C^{\gamma}$ s(15), H^{α} b2(11), $C^{\gamma}C^{\delta}$ s(11)
		1359 W		1368	$C^{\beta}H_2$ w(38), $C^{\gamma}H_2$ w(17), $C^{\beta}C^{\gamma}$ s(15), H^{α} b2(11), $C^{\gamma}C^{\delta}$ s(11)

(*continued*)

TABLE II (*continued*)

Observed[a]			Calculated				
Wet	Dry						
Raman	Raman	ir	A	B_1	B_2	B_3	Potential Energy Distribution[b]
					1339		$C^{\beta}H_2$ tw(31), NH ib(13), $C^{\gamma}H_2$ tw(12), H^{α} b2(10)
						1338	$C^{\beta}H_2$ tw(33), $C^{\gamma}H_2$ tw(13), NH ib(12), H^{α} b2(10)
1324 M	1321 M		1330				$C^{\beta}H_2$ tw(44), $C^{\gamma}H_2$ tw(28)
		1323 M		1330			$C^{\beta}H_2$ tw(44), $C^{\gamma}H_2$ tw(28)
					1319		$C^{\gamma}H_2$ tw(19), $C^{\beta}H_2$ tw(14), NH ib(13), H^{α} b2(11)
						1318	$C^{\gamma}H_2$ tw(18), H^{α} b2(14), NH ib(13), $C^{\beta}H_2$ tw(13), $C^{\gamma}H_2$ w(10)
					1306		H^{α} b2(37), CN s(16), CO ib(13)
						1305	H^{α} b2(34), CN s(17), CO ib(14)
1288 M	1287 M		1290				$C^{\gamma}H_2$ w(60), $C^{\gamma}C^{\delta}$ s(13), H^{α} b1(11), $C^{\beta}H_2$ w(10)
				1290			$C^{\gamma}H_2$ w(60), $C^{\gamma}C^{\delta}$ s(13), H^{α} b1(11), $C^{\beta}H_2$ w(10)
					1288		$C^{\gamma}H_2$ w(52), H^{α} b2(16), $C^{\beta}H_2$ w(11), $C^{\gamma}C^{\delta}$ s(11)
		1292 W				1288	$C^{\gamma}H_2$ w(52), H^{α} b2(15), $C^{\beta}H_2$ w(11), $C^{\gamma}C^{\delta}$ s(11)
1259 M	1260 M		1249				H^{α} b2(23), NC^{α} s(17), CN s(15), $C^{\gamma}H_2$ tw(14), NH ib(11)
		1260 MW		1248			H^{α} b2(21), NC^{α} s(18), CN s(15), $C^{\gamma}H_2$ tw(15), NH ib(10)
1222 M	1223 M		1222				H^{α} b2(22), $C^{\beta}H_2$ tw(16), $C^{\gamma}H_2$ tw(15), NH ib(11), NC^{α} s(10)
		1225 sh		1221			H^{α} b2(23), $C^{\beta}H_2$ tw(16), $C^{\gamma}H_2$ tw(14), NH ib(12)
					1210		$C^{\gamma}H_2$ tw(38), $C^{\beta}H_2$ tw(37)
1190 M	1187 M	1187MW	}			1210	$C^{\gamma}H_2$ tw(38), $C^{\beta}H_2$ tw(37)
1175 M	1176 W sh		1160				H^{α} b1(33), $C^{\beta}H_2$ w(16), NC^{α} s(14), $C^{\gamma}H_2$ tw(13)
				1159			H^{α} b1(33), $C^{\beta}H_2$ w(16), NC^{α} s(14), $C^{\gamma}H_2$ tw(12)
					1134		H^{α} b1(56), $C^{\beta}H_2$ w(26)
						1134	H^{α} b1(56), $C^{\beta}H_2$ w(26)
1125 W	1123 W		1121				H^{α} b1(28), NC^{α} s(18), $C^{\gamma}H_2$ tw(17), $C^{\beta}H_2$ w(13)
		1130 M		1121			H^{α} b1(28), NC^{α} s(18), $C^{\gamma}H_2$ tw(17), $C^{\beta}H_2$ w(13)

				1111	$C^{\alpha}C^{\beta}$ s(39), NC^{α} s(21)
				1111	$C^{\alpha}C^{\beta}$ s(39), NC^{α} s(21)
1066 VS	1066 VS		1062		$C^{\alpha}C^{\beta}$ s(31), $C^{\beta}C^{\gamma}$ s(30)
				1062	$C^{\alpha}C^{\beta}$ s(31), $C^{\beta}C^{\gamma}$ s(30)
				1061	$C^{\beta}C^{\gamma}$ s(29), $C^{\beta}H_2$ r(12), $C^{\alpha}C^{\beta}$ s(11)
		1074 VW		1061	$C^{\beta}C^{\gamma}$ s(30), $C^{\beta}H_2$ r(11), $C^{\alpha}C^{\beta}$ s(11)
				1042	$C^{\beta}C^{\gamma}$ s(30), $C^{\alpha}C^{\beta}$ s(11), $C^{\beta}H_2$ r(11)
1050 VW sh	1050 W sh			1041	$C^{\beta}C^{\gamma}$ s(28), $C^{\beta}H_2$ r(12), $C^{\alpha}C^{\beta}$ s(11)
			1040		$C^{\alpha}C^{\beta}$ s(41), $C^{\beta}C^{\gamma}$ s(30)
		1040 VW		1040	$C^{\alpha}C^{\beta}$ s(41), $C^{\beta}C^{\gamma}$ s(30)
1011 M	1015 W		1003		$C^{\gamma}C^{\delta}$ s(27)
		~1018 VW		1001	$C^{\gamma}C^{\delta}$ s(28)
				999	$C^{\gamma}C^{\delta}$ s(29)
				998	$C^{\gamma}C^{\delta}$ s(29)
			979		$C^{\gamma}H_2$ r(28), NC^{α} s(15), $C^{\beta}H_2$ r(13), $C^{\beta}H_2$ tw(11)
				979	$C^{\gamma}H_2$ r(28), NC^{α} s(15), $C^{\beta}H_2$ r(13), $C^{\beta}H_2$ tw(11)
		957 M,br		945	NC^{α} s(26), $C^{\gamma}H_2$ r(18)
956 S	956 S		944		$C^{\alpha}C$ s(18), CN s(13), CO s(11), $C^{\gamma}C^{\delta}$ s(10)
		943 VW sh		943	NC^{α} s(27), $C^{\gamma}H_2$ r(17)
938 sh				936	$C^{\alpha}C$ s(19), CN s(14), CO s(12), CNC^{α} d(10)
				896	$C^{\alpha}C$ s(42), CN s(10)
901 W	899 W	891 W		893	$C^{\alpha}C$ s(42), CN s(11)
				819	$C^{\beta}H_2$ r(28), $C^{\gamma}H_2$ r(24), CO ib(11)
				815	$C^{\beta}H_2$ r(29), $C^{\gamma}H_2$ r(22), CO ib(12)
798 W	798 W		804		$C^{\beta}H_2$ r(53), $C^{\gamma}H_2$ r(34)
		797 W		804	$C^{\beta}H_2$ r(53), $C^{\gamma}H_2$ r(34)
				776	NC^{α} s(22), $C^{\beta}H_2$ r(22), CO ib(14)
770 W	768 W	~765 VW[e]		776	NC^{α} s(23), $C^{\beta}H_2$ r(21), CO ib(14)
				731	CN t(50), NH ob(20)
			730		$C^{\delta}O_2$ b(38), $C^{\delta}O_2$ ss(12)
		723 W		728	$C^{\delta}O_2$ b(40), $C^{\delta}O_2$ ss(13)

(*continued*)

TABLE II (*continued*)

Observed[a]			Calculated				
Wet	Dry						
Raman	Raman	ir	A	B_1	B_2	B_3	Potential Energy Distribution[b]
						726	CN t(36), $C^{\delta}O_2$ b(17), NH ob(15)
				718			CN t(34), NH ob(31), CO ob(11)
705 VW			713				CN t(42), NH ob(31)
					710		$C^{\delta}O_2$ b(35), CN t(14), $C^{\delta}O_2$ ss(11)
						704	CN t(35), $C^{\delta}O_2$ b(25), NH ob(15)
			682				CO ob(24), CO ib(19), CN t(17)
				671			CN t(25), CO ib(21), CO ob(13), $C^{\delta}O_2$ w(10)
			653				CO ob(38), CO ib(20), C^{β} b1(12)
		653 S,br		648			CO ob(39), CO ib(19), C^{β} bl(13)
625 VW					629		$C^{\alpha}CN$ d(22), $C^{\delta}O_2$ w(19), NH ob(13), CO ob(11), C^{β} b2(10)
						629	CO ob(28), $C^{\alpha}CN$ d(19), NH ob(17), $C^{\delta}O_2$ w(14), C^{β} b2(12)
						616	CO ob(38), $C^{\delta}O_2$ w(27), $C^{\delta}O_2$ b(10)
					613		CO ob(46), $C^{\delta}O_2$ w(20), NH ob(10)
			606				$C^{\delta}O_2$ w(51), $C^{\delta}O_2$ b(11), CO ob(10)
				605			$C^{\delta}O_2$ w(49), CO ob(12), $C^{\delta}O_2$ b(10)
					581		CO ob(28), $C^{\alpha}CN$ d(24), $C^{\delta}O_2$ w(16)
						578	$C^{\alpha}CN$ d(30), CO ob(21), $C^{\delta}O_2$ w(14)
			502				$C^{\delta}O_2$ r(85)
				502			$C^{\delta}O_2$ r(86)
					499		$C^{\delta}O_2$ r(89)
						498	$C^{\delta}O_2$ r(89)
					450		C^{β} b1(45), NH ob(12)
						450	C^{β} b1(44), NH ob(12)
			433				C^{β} b2(51), $NC^{\alpha}C$ d(14)
				433			C^{β} b2(50), $NC^{\alpha}C$ d(14)

		377			C^{β} b2(20), $C^{\alpha}CN$ d(14), $C^{\alpha}C^{\beta}C^{\gamma}$ d(14)
			377		C^{β} b2(21), $C^{\alpha}CN$ d(14), $C^{\alpha}C^{\beta}C^{\gamma}$ d(14)
333 W	334 W		310		$NC^{\alpha}C$ d(28), $C^{\alpha}CN$ d(17), $C^{\alpha}C^{\beta}C^{\gamma}$ d(11)
301 W	297 W	304			$NC^{\alpha}C$ d(29), $C^{\alpha}CN$ d(15), $C^{\alpha}C^{\beta}C^{\gamma}$ d(13), CO ib(12)
				299	CO ib(31), $NC^{\alpha}C$ d(15), $C^{\alpha}C^{\beta}C^{\gamma}$ d(14), $C^{\alpha}C$ s(10)
				297	CO ib(30), $C^{\alpha}C^{\beta}C^{\gamma}$ d(16), $NC^{\alpha}C$ d(15), $C^{\alpha}C$ s(10)
				278	$C^{\alpha}C^{\beta}C^{\gamma}$ d(23), C^{β} b1(16), C^{β} b2(12)
				272	$C^{\alpha}C^{\beta}C^{\gamma}$ d(21), C^{β} b1(15), C^{β} b2(14), $C^{\beta}C^{\gamma}C^{\delta}$ d(10)
				255	C^{β} b2(27), CNC^{α} d(14), CO ib(10)
				254	C^{β} b2(25), CNC^{α} d(14)
			235		CNC^{α} d(18), $C^{\alpha}C^{\beta}C^{\gamma}$ d(16), $C^{\alpha}CN$ d(14)
	210 W(?)	213			CNC^{α} d(18), $C^{\alpha}C^{\beta}C^{\gamma}$ d(16), $C^{\alpha}CN$ d(14)
			204		C^{β} b1(20), NH ob(18)
				181	$C^{\beta}C^{\gamma}C^{\delta}$ d(34), H · · · O s(12)
		179			CNC^{α} d(42), C^{β} b1(11)
				175	$C^{\beta}C^{\gamma}C^{\delta}$ d(40), $C^{\alpha}C^{\beta}C^{\gamma}$ d(13), $C^{\delta}O_2$ w(10)
			150		$C^{\beta}C^{\gamma}C^{\delta}$ d(21), $C^{\gamma}C^{\delta}$ t(19)
		147			$C^{\gamma}C^{\delta}$ t(23), $C^{\beta}C^{\gamma}C^{\delta}$ d(18), NH ob(11), C^{β} b1(10)
			131		$C^{\gamma}C^{\delta}$ t(34), $C^{\beta}C^{\gamma}C^{\delta}$ d(22), $C^{\alpha}C^{\beta}C^{\gamma}$ d(15), $NC^{\alpha}C$ d(11)
		130			$C^{\gamma}C^{\delta}$ t(32), $C^{\beta}C^{\gamma}C^{\delta}$ d(26), $C^{\alpha}C^{\beta}C^{\gamma}$ d(11), $NC^{\alpha}C$ d(10)
				130	H · · · O s(19), CO · · · H t(18), CN t(17), NH ob(11)
				117	H · · · O s(41), $C^{\gamma}C^{\delta}$ t(33)
			112		CO · · · H t(17), CN t(14), NC^{α} s(10)
				112	$C^{\gamma}C^{\delta}$ t(64)
				98	$C^{\gamma}C^{\delta}$ t(27), H · · · O s(13), CO · · · H t(11)
		96			NH ob(17), $C^{\gamma}C^{\delta}$ t(16), $C^{\alpha}C^{\beta}C^{\gamma}$ d(15), $NC^{\alpha}C$ d(12), $C^{\beta}C^{\gamma}$ t(10)
			95		$C^{\gamma}C^{\delta}$ t(22), NH ob(17), $C^{\beta}C^{\gamma}$ t(14), CO ob(10)
		81			C^{β} b1(23), CO · · · H t(12), $C^{\alpha}C$ t(11)
				72	$C^{\alpha}C$ t(28), NC^{α} t(14), CO · · · H t(14), $C^{\beta}C^{\gamma}$ t(11)

(*continued*)

TABLE II (*continued*)

Observed[a]			Calculated				
Wet	Dry						
Raman	Raman	ir	A	B_1	B_2	B_3	Potential Energy Distribution[b]
			41				NH · · · O ib(23), $C^{\alpha}C^{\beta}$ t(18), CO · · · H ib(12), NH · · · O t(10), H · · · O s(10)
					36		$C^{\alpha}C^{\beta}$ t(46), $C^{\beta}C^{\gamma}$ t(32), $C^{\gamma}C^{\delta}$ t(12)
						36	$C^{\alpha}C^{\beta}$ t(50), $C^{\beta}C^{\gamma}$ t(33), $C^{\gamma}C^{\delta}$ t(12)
				35			$C^{\alpha}C^{\beta}$ t(55), $C^{\beta}C^{\gamma}$ t(27), $C^{\gamma}C^{\delta}$ t(13)
			34				$C^{\beta}C^{\gamma}$ t(41), $C^{\alpha}C^{\beta}$ t(35)
					34		CO · · · H t(27), NC^{α} t(11), $NC^{\alpha}C$ d(11), NH · · · O t(11), NH ob(10)
					26		CN t(31), NH · · · O t(22), CO · · · H t(12), $NC^{\alpha}C$ d(12)
				24			$C^{\beta}C^{\gamma}$ t(43), $C^{\alpha}C^{\beta}$ t(18)
						24	$NC^{\alpha}C$ d(19), $C^{\alpha}C^{\beta}C^{\gamma}$ d(12), CNC^{α} d(11), $C^{\beta}C^{\gamma}$ t(10)
					18		$C^{\beta}C^{\gamma}$ t(41), $C^{\alpha}C^{\beta}$ t(28)
			17				$C^{\beta}C^{\gamma}$ t(31), $C^{\alpha}C^{\beta}$ t(23), NH · · · O ib(11)
						17	$C^{\beta}C^{\gamma}$ t(36), $C^{\alpha}C^{\beta}$ t(30)
				13			NH · · · O t(20), NH ob(14), CO · · · H t(12), C^{β} b1(12)
			8				CO · · · H t(35), H · · · O s(12), NH · · · O t(11)

[a] S = strong, M = medium, W = weak, V = very, sh = shoulder, br = broad.

[b] s = stretch, as = antisymmetric stretch, ss = symmetric stretch, b = angle bend, ib = in-plane angle bend, ob = out-of-plane angle bend, w = wag, r = rock, tw = twist, d = deformation, t = torsion. Only contributions of 10% or greater are included.

[c] Observed (perturbed by Fermi resonance) frequency.

[d] Unperturbed frequency.

[e] Observed at liquid N_2 temperature.

TABLE III
Observed and Calculated Frequencies (cm^{-1}) of β-(GluCa–ND)$_n$

Observed[a]			Calculated				
Wet	Dry						
Raman	Raman	ir	A	B_1	B_2	B_3	Potential Energy Distribution[b]
2982 MW			2982				$C^{\gamma}H_2$ as(99)
		~2965 W		2982			$C^{\gamma}H_2$ as(99)
					2982		$C^{\gamma}H_2$ as(99)
						2982	$C^{\gamma}H_2$ as(99)
2940 S			2943				$C^{\gamma}H_2$ ss(99)
				2943			$C^{\gamma}H_2$ ss(99)
		~2932W			2943		$C^{\gamma}H_2$ ss(99)
						2943	$C^{\gamma}H_2$ ss(99)
2919 VS			2918				$C^{\beta}H_2$ as(99)
				2918			$C^{\beta}H_2$ as(99)
					2918		$C^{\beta}H_2$ as(99)
						2918	$C^{\beta}H_2$ as(99)
2876 W			2877				$C^{\alpha}H^{\alpha}$ s(96)
						2877	$C^{\alpha}H^{\alpha}$ s(96)
				2867			$C^{\alpha}H^{\alpha}$ s(93)
		~2872 W,br			2867		$C^{\alpha}H^{\alpha}$ s(93)
			2855				$C^{\beta}H_2$ ss(97)
				2855			$C^{\beta}H_2$ ss(93)
					2855		$C^{\beta}H_2$ ss(93)
						2855	$C^{\beta}H_2$ ss(97)
			2382				ND s(96)
				2382			ND s(96)
		2421[c]			2382		ND s(96)
						2382	ND s(96)

(*continued*)

TABLE III (*continued*)

Observed[a]			Calculated				
Wet	Dry						
Raman	Raman	ir	A	B_1	B_2	B_3	Potential Energy Distribution[b]
						1696	CO s(70), CN s(18)
		1687 W		1689			CO s(72), CN s(21)
1656 S			1664				CO s(72), CN s(20)
		1620 VS			1625		CO s(70), CN s(18)
1556 W			1561				$C^{\delta}O_2$ as(87)
		1560 VS		1561			$C^{\delta}O_2$ as(87)
					1561		$C^{\delta}O_2$ as(87)
						1561	$C^{\delta}O_2$ as(87)
		1469 W		1486			$C^{\alpha}C$ s(23), CN s(23), CO ib(16)
1459 S			1485				$C^{\alpha}C$ s(23), CN s(23), CO ib(15), CO s(10), $C^{\beta}H_2$ b(10)
						1483	$C^{\alpha}C$ s(24), CN s(21), CO ib(14), H^{α} b2(11)
					1483		$C^{\alpha}C$ s(24), CN s(20), CO ib(13), H^{α} b2(12)
					1458		$C^{\beta}H_2$ b(48), $C^{\gamma}H_2$ b(42)
						1458	$C^{\beta}H_2$ b(49), $C^{\gamma}H_2$ b(42)
			1457				$C^{\gamma}H_2$ b(54), $C^{\beta}H_2$ b(36)
1448 M				1457			$C^{\gamma}H_2$ b(54), $C^{\beta}H_2$ b(36)
					1446		$C^{\gamma}H_2$ b(51), $C^{\beta}H_2$ b(33)
		1440 S,br				1446	$C^{\gamma}H_2$ b(51), $C^{\beta}H_2$ b(33)
			1445				$C^{\beta}H_2$ b(43), $C^{\gamma}H_2$ b(39)
				1445			$C^{\beta}H_2$ b(43), $C^{\gamma}H_2$ b(39)
1424 S			1416				$C^{\delta}O_2$ ss(58), $C^{\delta}O_2$ b(21), $C^{\gamma}C^{\delta}$ s(13)
				1416			$C^{\delta}O_2$ ss(58), $C^{\delta}O_2$ b(21), $C^{\gamma}C^{\delta}$ s(13)
					1416		$C^{\delta}O_2$ ss(57), $C^{\delta}O_2$ b(21), $C^{\gamma}C^{\delta}$ s(14)
		1414 S				1416	$C^{\delta}O_2$ ss(58), $C^{\delta}O_2$ b(21), $C^{\gamma}C^{\delta}$ s(14)
1386 W			1380				$C^{\beta}H_2$ w(49), $C^{\beta}C^{\gamma}$ s(16)
				1380			$C^{\beta}H_2$ w(49), $C^{\beta}C^{\gamma}$ s(16)

1375 VW			1379		$C^{\beta}H_2$ w(46), $C^{\beta}C^{\gamma}$ s(17), $C^{\alpha}C^{\beta}$ s(10)
			1379		$C^{\beta}H_2$ w(46), $C^{\beta}C^{\gamma}$ s(17), $C^{\alpha}C^{\beta}$ s(10)
1353 W		1346			H^{α} b2(41), $C^{\beta}H_2$ tw(22)
1363 W	~1360 W		1346		H^{α} b2(42), $C^{\beta}H_2$ tw(22)
1338 W				1330	$C^{\beta}H_2$ tw(42), $C^{\gamma}H_2$ tw(29)
1334 W				1330	$C^{\beta}H_2$ tw(42), $C^{\gamma}H_2$ tw(29)
1314 M		1322			$C^{\gamma}H_2$ tw(24), $C^{\beta}H_2$ tw(23), H^{α} b2(22)
	1320 M		1322		$C^{\gamma}H_2$ tw(24), $C^{\beta}H_2$ tw(23), H^{α} b2(23)
				1308	H^{α} b2(43), $C^{\gamma}H_2$ w(24)
				1308	H^{α} b2(43), $C^{\gamma}H_2$ w(24)
1288 M		1289			$C^{\gamma}H_2$ w(56), $C^{\gamma}C^{\delta}$ s(13), H^{α} b2(11), H^{α} b1(11)
			1289		$C^{\gamma}H_2$ w(57), $C^{\gamma}C^{\delta}$ s(13), H^{α} b2(11), H^{α} b1(11)
				1288	$C^{\gamma}H_2$ w(45), H^{α} b2(26), H^{α} b1(10), $C^{\gamma}C^{\delta}$ s(10)
	1287 W			1288	$C^{\gamma}H_2$ w(44), H^{α} b2(27), H^{α} b1(10), $C^{\gamma}C^{\delta}$ s(10)
1231 W		1227			$C^{\gamma}H_2$ tw(29), $C^{\beta}H_2$ tw(27), NC^{α} s(19)
	1237 M		1227		$C^{\gamma}H_2$ tw(29), $C^{\beta}H_2$ tw(27), NC^{α} s(19)
				1212	$C^{\gamma}H_2$ tw(41), $C^{\beta}H_2$ tw(40)
1189 M	1187 MW			1212	$C^{\gamma}H_2$ tw(41), $C^{\beta}H_2$ tw(40)
1155 W				1163	H^{α} b1(48), $C^{\beta}H_2$ w(26), ND ib(12)
				1163	H^{α} b1(49), $C^{\beta}H_2$ w(26), ND ib(12)
1173 W		1159			H^{α} b1(35), $C^{\beta}H_2$ w(17), NC^{α} s(13), $C^{\gamma}H_2$ tw(11)
			1159		H^{α} b1(35), $C^{\beta}H_2$ w(17), NC^{α} s(13), $C^{\gamma}H_2$ tw(11)
1122 W		1118			H^{α} b1(28), NC^{α} s(19), $C^{\gamma}H_2$ tw(16), $C^{\beta}H_2$ w(12)
	1130 M		1118		H^{α} b1(27), NC^{α} s(19), $C^{\gamma}H_2$ tw(16), $C^{\beta}H_2$ w(12)
				1109	$C^{\alpha}C^{\beta}$ s(40), NC^{α} s(20)
				1109	$C^{\alpha}C^{\beta}$ s(40), NC^{α} s(20)
				1072	ND ib(17), $C^{\beta}H_2$ r(17), $C^{\gamma}H_2$ r(12), $C^{\gamma}H_2$ tw(10)
				1072	ND ib(17), $C^{\beta}H_2$ r(17), $C^{\gamma}H_2$ r(12)
1067 VS		1062			$C^{\beta}C^{\gamma}$ s(31), $C^{\alpha}C^{\beta}$ s(30)

(*continued*)

TABLE III (*continued*)

Observed[a]			Calculated				
Wet	Dry						
Raman	Raman	ir	A	B_1	B_2	B_3	Potential Energy Distribution[b]
				1062			$C^{\alpha}C^{\beta}$ s(31), $C^{\beta}C^{\gamma}$ s(30)
					1058		$C^{\beta}C^{\gamma}$ s(55)
		~1074 VW				1058	$C^{\beta}C^{\gamma}$ s(56)
			1052				ND ib(37), $C^{\alpha}C$ s(16)
1041 W				1050			ND ib(38), $C^{\alpha}C$ s(16)
			1039				$C^{\alpha}C^{\beta}$ s(42), $C^{\beta}C^{\gamma}$ s(29)
		~1040 VW		1039			$C^{\alpha}C^{\beta}$ s(42), $C^{\beta}C^{\gamma}$ s(29)
					1008		$C^{\gamma}C^{\delta}$ s(23), ND ib(11)
						1008	$C^{\gamma}C^{\delta}$ s(24), ND ib(10)
1009 W			996				$C^{\gamma}C^{\delta}$ s(22), $C^{\gamma}H_2$ r(16)
				995			$C^{\gamma}C^{\delta}$ s(23), $C^{\gamma}H_2$ r(16)
					977		ND ib(32), $C^{\beta}C^{\gamma}$ s(13), $C^{\gamma}C^{\delta}$ s(10), H^{α} b1(10)
992 VS						976	ND ib(33), $C^{\beta}C^{\gamma}$ s(13), H^{α} b1(10)
950 M			966				$C^{\gamma}H_2$ r(18), $C^{\gamma}C^{\delta}$ s(15), NC^{α} s(13)
		948 M		966			$C^{\gamma}H_2$ r(18), $C^{\gamma}C^{\delta}$ s(14), NC^{α} s(13)
					935		NC^{α} s(32), $C^{\gamma}H_2$ r(16)
936 sh		940 VW sh				934	NC^{α} s(32), $C^{\gamma}H_2$ r(13)
913 W			910				CN s(20), ND ib(18), $C^{\alpha}C$ s(13), CO s(12)
				902			CN s(20), ND ib(16), $C^{\alpha}C$ s(13), CO s(13)
898 VW		~889 W			893		$C^{\alpha}C$ s(41), CN s(12)
						890	$C^{\alpha}C$ s(39), CN s(13), $C^{\gamma}H_2$ r(10)
					814		$C^{\beta}H_2$ r(32), $C^{\gamma}H_2$ r(24)
						809	$C^{\beta}H_2$ r(33), $C^{\gamma}H_2$ r(22)
794 VW,br			803				$C^{\beta}H_2$ r(53), $C^{\gamma}H_2$ r(33)
		~795 W		803			$C^{\beta}H_2$ r(53), $C^{\gamma}H_2$ r(33)

				766	NC^{α} s(22), $C^{\beta}H_2$ r(17), CO ib(15)
~755 sh			765		NC^{α} s(22), $C^{\beta}H_2$ r(19), CO ib(14)
	727				$C^{\delta}O_2$ b(41), $C^{\delta}O_2$ ss(13), $C^{\beta}C^{\gamma}C^{\delta}$ d(10)
~723 W		726			$C^{\delta}O_2$ b(41), $C^{\delta}O_2$ ss(13), $C^{\beta}C^{\gamma}C^{\delta}$ d(11), $C^{\delta}O_2$ w(10)
			715		$C^{\delta}O_2$ b(42), $C^{\delta}O_2$ ss(13), $C^{\beta}C^{\gamma}C^{\delta}$ d(13), $C^{\delta}O_2$ w(13)
				715	$C^{\delta}O_2$ b(42), $C^{\delta}O_2$ ss(14), $C^{\beta}C^{\gamma}C^{\delta}$ d(13), $C^{\delta}O_2$ w(12)
	686				CO ob(35), CO ib(19)
		686			CO ob(40), CO ib(16)
	649				CO ob(30), CO ib(25)
~645 S,br		645			CO ib(31), CO ob(25)
			634		CO ob(37), $C^{\alpha}CN$ d(13), $C^{\delta}O_2$ w(12)
				630	CO ob(36), $C^{\delta}O_2$ w(15), $C^{\alpha}CN$ d(13)
			617		CO ob(34), $C^{\delta}O_2$ w(28), $C^{\delta}O_2$ b(10)
630 W				616	CO ob(38), $C^{\delta}O_2$ w(27)
	606				$C^{\delta}O_2$ w(51), $C^{\delta}O_2$ b(11)
		606			$C^{\delta}O_2$ w(50), $C^{\delta}O_2$ b(12)
			572		$C^{\alpha}CN$ d(33), $C^{\delta}O_2$ w(14), CO ob(13)
~593 W				568	$C^{\alpha}CN$ d(34), CO ob(15), $C^{\delta}O_2$ w(13)
			521		CN t(44), ND ob(35)
	519				CN t(52), ND ob(25), ND · · · O t(10)
534 W				515	CN t(48), ND ob(34), ND · · · O ib(10)
531 M		506			CN t(50), ND ob(21), $C^{\delta}O_2$ r(16)
	501				$C^{\delta}O_2$ r(85)
		501			$C^{\delta}O_2$ r(68), CN t(17), ND ob(10)
			498		$C^{\delta}O_2$ r(89)
				498	$C^{\delta}O_2$ r(89)
			447		C^{β} b1(44)
				447	C^{β} b1(42)
	430				C^{β} b2(48), $NC^{\alpha}C$ d(14)
		430			C^{β} b2(47), $NC^{\alpha}C$ d(13)

(continued)

TABLE III (*continued*)

Observed[a]			Calculated				
Wet	Dry						
Raman	Raman	ir	A	B_1	B_2	B_3	Potential Energy Distribution[b]
			375				C^{β} b2(22), $C^{\alpha}C^{\beta}C^{\gamma}$ d(13), $C^{\alpha}CN$ d(12)
				375			C^{β} b2(24), $C^{\alpha}CN$ d(13), $C^{\alpha}C^{\beta}C^{\gamma}$ d(13)
				308			$NC^{\alpha}C$ d(29), $C^{\alpha}CN$ d(17), $C^{\alpha}C^{\beta}C^{\gamma}$ d(12)
300 W			302				$NC^{\alpha}C$ d(29), $C^{\alpha}CN$ d(15), $C^{\alpha}C^{\beta}C^{\gamma}$ d(14), CO ib(12)
					298		CO ib(30), $C^{\alpha}C^{\beta}C^{\gamma}$ d(16), $NC^{\alpha}C$ d(14), $C^{\alpha}C$ s(10)
						297	CO ib(29), $C^{\alpha}C^{\beta}C^{\gamma}$ d(18), $NC^{\alpha}C$ d(14), $C^{\alpha}C$ s(10)
						275	$C^{\alpha}C^{\beta}C^{\gamma}$ d(20), C^{β} b1(15), C^{β} b2(14)
					268		$C^{\alpha}C^{\beta}C^{\gamma}$ d(18), C^{β} b2(17), C^{β} b1(14), $C^{\beta}C^{\gamma}C^{\delta}$ d(11)
						255	C^{β} b2(25), CNC^{α} d(15), CO ib(10)
					254		C^{β} b2(22), CNC^{α} d(15), $C^{\alpha}C^{\beta}C^{\gamma}$ d(11)
				233			CNC^{α} d(32), D · · · O s(24), $C^{\alpha}CN$ d(13)
			210				CNC^{α} d(19), $C^{\alpha}CN$ d(15), $C^{\alpha}C^{\beta}C^{\gamma}$ d(15)
				201			C^{β} b1(20), ND ob(15)
			176				CNC^{α} d(41), C^{β} 1(11)
						180	$C^{\beta}C^{\gamma}C^{\delta}$ d(35), D · · · O s(12)
					174		$C^{\beta}C^{\gamma}C^{\delta}$ d(40), $C^{\alpha}C^{\beta}C^{\gamma}$ d(13), $C^{b}O_2$ w(10)
				150			$C^{\beta}C^{\gamma}C^{\delta}$ d(22), $C^{\gamma}C^{\delta}$ t(19)
			147				$C^{\gamma}C^{\delta}$ t(22), $C^{\beta}C^{\gamma}C^{\delta}$ d(19), ND ob(11)
				131			$C^{\gamma}C^{\delta}$ t(35), $C^{\beta}C^{\gamma}C^{\delta}$ d(22), $C^{\alpha}C^{\beta}C^{\gamma}$ d(14), $NC^{\alpha}C$ d(11)
			130				$C^{\gamma}C^{\delta}$ t(33), $C^{\beta}C^{\gamma}C^{\delta}$ d(25), $C^{\alpha}C^{\beta}C^{\gamma}$ d(11), $NC^{\alpha}C$ d(10)
						129	CO · · · D t(18), D · · · O s(18), CN t(16), ND ob(10)
						116	D · · · O s(42), $C^{\gamma}C^{\delta}$ t(33)
					112		$C^{\gamma}C^{\delta}$ t(65)
				111			CO · · · D t(17), CN t(13), NC^{α} s(10)
						97	$C^{\gamma}C^{\delta}$ t(26), D · · · O s(13), CO · · · D t(11)
			96				ND ob(18), $C^{\gamma}C^{\delta}$ t(16), $C^{\alpha}C^{\beta}C^{\gamma}$ d(14), $NC^{\alpha}C$ d(13), $C^{\beta}C^{\gamma}$ t(10)

	95			$C^{\gamma}C^{\delta}$ t(22), ND ob(17), $C^{\beta}C^{\gamma}$ t(14), CO ob(10)
81				C^{β} b1(23), CO · · · D t(12), $C^{\alpha}C$ t(11)
		71		$C^{\alpha}C$ t(28), NC^{α} t(15), CO · · · D t(14), $C^{\beta}C^{\gamma}$ t(11)
41				ND · · · O ib(23), $C^{\alpha}C^{\beta}$ t(18), CO · · · D ib(12), ND · · · O t(10), D · · · O s(10)
		36		$C^{\alpha}C^{\beta}$ t(46), $C^{\beta}C^{\gamma}$ t(32), $C^{\gamma}C^{\delta}$ t(12)
			36	$C^{\alpha}C^{\beta}$ t(50), $C^{\beta}C^{\gamma}$ t(33), $C^{\gamma}C^{\delta}$ t(12)
	35			$C^{\alpha}C^{\beta}$ t(55), $C^{\beta}C^{\gamma}$ t(27), $C^{\gamma}C^{\delta}$ t(13)
		34		CO · · · D t(27), $NC^{\alpha}C$ d(12), NC^{α} t(11), ND · · · O t(11), ND ob(10)
34				$C^{\beta}C^{\gamma}$ t(42), $C^{\alpha}C^{\beta}$ t(34)
		26		CN t(31), ND · · · O t(23), CO · · · D t(13), $NC^{\alpha}C$ d(12)
	24			$C^{\beta}C^{\gamma}$ t(42), $C^{\alpha}C^{\beta}$ t(18)
			24	$NC^{\alpha}C$ d(19), $C^{\alpha}C^{\beta}C^{\gamma}$ d(12), CNC^{α} d(11), $C^{\beta}C^{\gamma}$ t(10)
		18		$C^{\beta}C^{\gamma}$ t(41), $C^{\alpha}C^{\beta}$ t(28)
17				$C^{\beta}C^{\gamma}$ t(31), $C^{\alpha}C^{\beta}$ t(23), ND · · · O ib(11)
			17	$C^{\beta}C^{\gamma}$ t(36), $C^{\alpha}C^{\beta}$ t(30)
	13			ND · · · O t(21), ND ob(14), CO · · · D t(12), C^{β} b1(12)
8				CO · · · D t(35), D · · · O s(12), ND · · · O t(11)

[a] S = strong, M = medium, W = weak, V = very, sh = shoulder, br = broad.

[b] s = stretch, as = antisymmetric stretch, ss = symmetric stretch, b = angle bend, ib = in-plane angle bend, ob = out-of-plane angle bend, w = *wag*, r = *rock*, *tw* = *twist*, *d* = *deformation*, *t* = *torsion*. Only contributions of 10% or greater are included.

[c] Unperturbed frequency.

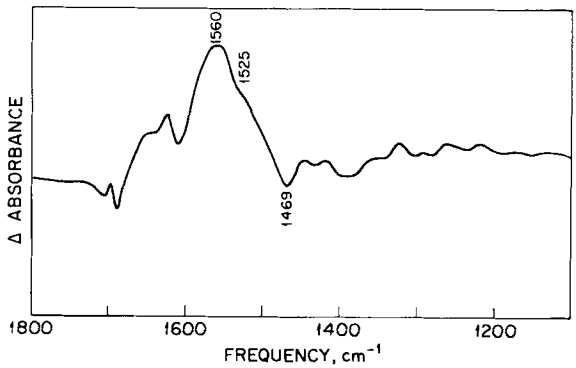

Fig. 9. Difference ir spectrum in the 1100–1800-cm^{-1} region, obtained by subtracting the spectrum of the N-deuterated derivative from that of the parent compound.

Fig. 9). At the present time, therefore, the B_1-species assignment must be considered uncertain. On N-deuteration there is a relative intensity decrease in the weak band at 1567 cm^{-1} in the Raman spectrum, the adjacent 1557 cm^{-1} COO^{-1} antisymmetric stretch band remaining almost constant; we believe that, as in β-$(Ala)_n$,[4] this band can be assigned to the B_2-species mode calculated at 1576 cm^{-1}. A weak Raman band at 1598 cm^{-1} may be assignable to the B_3-species mode, calculated at 1607 cm^{-1}. An amide II′ mode, which appears as a new band in the Raman spectrum of β-$(GluCa–ND)_n$ at 1459 cm^{-1} and, as we have seen, is expected near this position from a Fermi resonance analysis, is calculated somewhat high. The ir difference spectrum shows the presence of a weak band at 1469 cm^{-1} in β-$(GluCa–ND)_n$, which can be assigned, as in the case of β-$(Ala–ND)_n$,[4] to the B_1-species amide II′ mode.

The COO^- antisymmetric and symmetric stretch modes, calculated at 1561 and 1416 cm^{-1}, respectively, of course, match the observed bands well because of the choice of force constants for the COO^- group.

The CH_2 bend modes are well accounted for, the $C^{\gamma}H_2$ modes apparently being more intense in the ir and Raman spectra than the $C^{\beta}H_2$ modes because of the adjacent COO^- group. The expected relative constancy in these frequencies is an added reason for assigning the new strong band at 1459 cm^{-1} in the Raman spectrum of β-$(GluCa–ND)_n$ to the amide II′ mode.

The 1200–1400 cm^{-1} region contains CH_2 wag and CH_2 twist modes mixed with various skeletal coordinates. Some bands remain constant on N-deuteration, as is predicted and observed for the modes near 1290 and 1190 cm^{-1} [which, as expected, are not present in β-$(Ala)_n$.][4] Others are predicted to shift on N-deuteration, and these shifts are observed: the A species H^{α} bend contribution is predicted to shift from 1414 cm^{-1} (where a weak shoulder is observed) to 1346 cm^{-1}, and a new band is

found at 1353 cm^{-1} in the Raman spectrum (a band at 1363 cm^{-1} is assigned to the B_1-species mode since a significant contribution from undeuterated material is excluded by the complete disappearance of the amide III mode at 1259 cm^{-1}; see below); $C^{\beta}H_2$ wag is predicted to shift its main A-species mode contribution from 1368 to 1380 cm^{-1}, and a new Raman band is found at 1386 cm^{-1}; and the predicted downward shift of the A-species $C^{\beta}H_2$ plus $C^{\gamma}H_2$ twist mode at 1330 cm^{-1} to a similar mode at 1322 cm^{-1} is mirrored by the downward shift of the observed 1324 cm^{-1} band to 1314 cm^{-1}. New weak bands appear in the Raman spectrum of the N-deuterated derivative at 1338 and 1334 cm^{-1}; these are probably assignable to the calculated B_2- and B_3-species modes at 1330 cm^{-1}, perhaps now exhibiting intensity owing to the loss of the NH in-plane bend contribution to the corresponding 1339 and 1338 cm^{-1} modes. Thus, subtle changes in side-chain vibrations that result from main-chain deuteration are predicted by the normal mode calculation and are observed in the spectra.

The amide III modes (CN stretch plus NH in-plane bend) are seen predominantly in the Raman spectrum in the 1200–1300 cm^{-1} region. These bands have been found to be sensitive to backbone conformation, but it also has been noted that the frequencies depend as well on side-chain composition.[25] In β-$(GluCa)_n$ the main amide III band occurs at 1259 cm^{-1} in the Raman spectrum, as is verified by its complete disappearance on N-deuteration. Its position and disappearance are well predicted. The Raman band at 1222 cm^{-1} can also be assigned to a mode with NH in-plane bend, but there is only a 5% contribution to the PED from CN stretch. On N-deuteration this band weakens and shifts upward to 1231 cm^{-1}, which is accounted for by the calculation. Similar changes are seen in the ir spectra, the 1260 and 1225 cm^{-1} bands being replaced by a band at 1237 cm^{-1} on N-deuteration. We correlate the weak ir band at ~1248 cm^{-1} with the weak Raman band at 1238 cm^{-1} that appears only in the spectrum of the dry sample, and we ascribe both of these to disordered structures. This conclusion is based on the observation that the rate of disappearance of the 1238 cm^{-1} band on deuteration is much faster than that of the nearby 1223 and 1260 cm^{-1} bands, consistent with a more rapid access of D_2O to the disordered regions. The amide III mode at 1259 cm^{-1} in β-$(GluCa)_n$ is to be compared with the equivalent mode at 1243 cm^{-1} in β-$(Ala)_n$,[4] where another mode of comparable PED is found at 1226 cm^{-1}, and that at 1236 cm^{-1} in β_{Γ}-$(GluH)_n$.[14] This emphasizes the point that the amide III frequency is sensitive to side-chain structure as well as backbone conformation,[25] and therefore, that caution must be exercised in using this band alone as a criterion of chain conformation.

A comment is in order about the components of amide II and amide III in the N-deuterated molecule. As we mentioned above, the CN stretch coordinate can be assigned to a new (amide II') Raman band at 1459 cm^{-1}, while the ND in-plane bend can be assigned to a new

Raman band at 992 cm^{-1}. Our calculation indicates that the ND in-plane bend should also contribute near 910 and 1052 cm^{-1}, and, in fact, new Raman bands are observed at 913 and 1041 cm^{-1}. However, since the latter modes are A and B_1 species, they cannot combine with the A or B_1 species amide II′ mode to give the B_2 species needed to interact by Fermi resonance with the B_2-species ND stretch mode. Nor are $1459(B_2,B_3) + 913(A,B_1) = 2372(B_2)$ or $1459(B_2,B_3) + 1041(A,B_1) = 2500(B_2)$ combinations close enough to $\nu_A^0 = 2421$ cm^{-1} to give a significant interaction. Thus, we observe only a Fermi resonance doublet, in contrast to the case of β-$(Ala–ND)_n$, where two ND in-plane bend modes are of the same symmetry and close enough in frequency so that both combinations with amide II′ can interact with ND stretch and give rise to a Fermi resonance triplet.[22] This analysis lends further support to our assignment of the 1459 cm^{-1} Raman band to an amide II′ mode.

The modes in the 900–1200 cm^{-1} region have major contributions from backbone and side-chain stretching. In most cases they are predicted, and observed, to remain relatively constant in frequency on N-deuteration; in others, shifts are predicted as a result of mixing with ND in-plane bend or because of a redistribution of PEDs, and these are observed. Thus, bands at 1175 R, 1130 ir, 1125 R, 1066 R, 1040 ir, and 901 R (~891 ir) are predicted and observed to remain essentially constant in frequency and character. The 1011 R band changes only slightly on N-deuteration. Changes occur in other modes for various reasons: unobserved H^{α}-bend modes calculated at 1134 cm^{-1} gain intensity and appear at 1155 cm^{-1} as a result of mixing with an ND in-plane bend; a weak shoulder at ~1050 cm^{-1} in the Raman spectrum disappears, apparently as a result of a redistribution of PED; and bands at 956 and 938 cm^{-1} shift slightly, again as a result of PED redistribution. The frequency and direction of shift are not always well predicted, but the qualitative aspects of the changes can be inferred with confidence. Of course, it must be remembered that this part of the force field was transferred without refinement from β-$(Ala)_n$.

Below 900 cm^{-1} our ir and Raman spectra show very few well-resolved bands. The 850 cm^{-1} Raman band, which is present in the spectrum of the dry sample but is noticeably absent from that of the wet crystals, and its probable counterpart at 843 cm^{-1} in the ir, are assigned to disordered structures. The weak bands at 798 R and 797 ir cm^{-1} are well assigned to CH_2 rock modes calculated at 804 cm^{-1}. The weak 770 R and 765 ir cm^{-1} bands can be assigned to NC^{α} stretch plus CO in-plane bend modes, as in β-$(Ala)_n$;[4] their predicted downward shift on N-deuteration seems to be observed in the ir. The C^5O_2 bend mode is predicted at 728 cm^{-1}, and may be assignable to the weak band near 723 cm^{-1}; this must be considered tentative since we have no experimental basis for refining the relevant force constants. Rather strangely, we can find no significant ir band that can be assigned to

the amide V mode (NH out-of-plane bend), which in β-$(Ala)_n$ is found as a strong band near 700 cm^{-1}. A weak Raman band at 705 cm^{-1} disappears on N-deuteration and can be assigned to amide V, but the potential candidate at 723 ir cm^{-1} persists and is therefore more likely to be the $C^{\delta}O_2$ bend mode. On the other hand, the strong, broad absorption at ~653 cm^{-1} in the ir, which persists on N-deuteration and is therefore presumably not due to H_2O (some of which is still present in dry crystals), can be assigned to a CO in-plane plus CO out-of-plane bend mode. Such a mixed mode does not occur in β-$(Ala)_n$,[4] where the individual modes are found to be weak. We recognize that $C^{\delta}O_2$ modes may also contribute in this region, and therefore these assignments must be considered tentative at present. Finally, we note that new bands at 531 ir and 534 R cm^{-1} in the N-deuterated derivative can readily be assigned to ND out-of-plane bend modes. They are well predicted by our calculation, comparable to those of β-$(Ala)_n$,[4] suggesting that our prediction for the amide V modes should be reasonably good.

CONCLUSIONS

The normal-mode calculations on β-$(GluCa)_n$ reproduce the observed ir and Raman bands quite well, the average error being 7 cm^{-1} for modes below 1700 cm^{-1}. This is despite the fact that main-chain force constants were transferred without refinement from β-$(Ala)_n$ and side-chain force constants were only slightly refined (to fit well-assigned bands) from the highly reliable force field for *n*-paraffins.[20] This analysis includes the explanation of rather subtle effects, such as the appearance of a single ν'_B mode as compared to the two in β-$(Ala\text{–}ND)_n$, and the small shifts in some modes on N-deuteration even though they do not contain significant contributions from NH motions.

These results thus not only confirm the proposed APPS structure for $(GluCa)_n$, which is slightly different from that of β-$(Ala)_n$, but they provide further insight into the influence of the side chain on the main-chain modes. Our detailed assignment of all the normal modes provides a clear basis for distinguishing main-chain vibrations from those due exclusively to the side chain, as well as permitting an identification of those bands which involve a mixing of main- and side-chain vibrations. The latter are perhaps best illustrated by the amide III mode in the Raman spectrum: no such assignable band is found in $(Gly\ I)_n$, with the calculated mode containing contributions from CO in-plane bend and $C^{\alpha}C$ stretch, in addition to large NH in-plane bend and CN stretch components; two bands are found in β-$(Ala)_n$ at 1243 S and 1226 M cm^{-1}, with the former two contributions absent and replaced by NC^{α} stretch and H^{α} bend components and the latter two contributions relatively diminished; and in β-$(GluCa)_n$ there are two bands at 1259 M and 1222 M cm^{-1}, but although the PEDS are similar

to those in β-(Ala)$_n$, there is a diminished contribution from NH in-plane bend and CN stretch but new contributions from $C^{\gamma}H_2$ and $C^{\beta}H_2$ twist. This reemphasizes our earlier observation[25] that amide III should not be used as an exclusive indicator of main-chain conformation.

Finally, the present study forms a reliable basis for the analysis of other conformations of poly(L-glutamic acid) and its salts (P. Sengupta and S. Krimm, to be published).

This research was supported by National Science Foundation Grants PCM-8214064 and DMR-8303610.

References

1. Krimm, S. (1983) *Biopolymers* **22**, 217–225.
2. Dwivedi, A. M. & Krimm, S. (1984) *Biopolymers* **23**, 923–943.
3. Dwivedi, A. M. & Krimm, S. (1982) *Macromolecules* **15**, 177–185.
4. Dwivedi, A. M. & Krimm, S. (1982) *Macromolecules* **15**, 186–197; (1983) *Macromolecules* **16**, 340.
5. Dwivedi, A. M. & Krimm, S. (1982) *Biopolymers* **21**, 2377–2397.
6. Lenormant, H., Baudras, A. & Blout, E. R. (1958) *J. Am. Chem. Soc.* **80**, 6191–6195.
7. Tiffany, M. L. & Krimm, S. (1968) *Biopolymers* **6**, 1379–1381.
8. Keith, H. D., Padden, F. J. & Giannoni, G. (1969) *J. Mol. Biol.* **43**, 423–438.
9. Keith, H. D., Giannoni, G. & Padden, F. J. (1969) *Biopolymers* **7**, 775–792.
10. Keith, H. D. (1970) *Biopolymers* **10**, 1099–1101.
11. Koenig, J. L. & Frushour, B. G. (1972) *Biopolymers* **11**, 1871–1892.
12. Zimmerman, S. S., Clark, J. C. & Mandelkern, L. (1975) *Biopolymers* **14**, 585–596.
13. Itoh, K., Foxman, B. M. & Fasman, G. D. (1976) *Biopolymers* **15**, 419–455.
14. Fasman, G. D., Itoh, K., Liu, C. S. & Lord, R. C. (1978) *Biopolymers* **17**, 1729–1746.
15. Hsu, S. L., Moore, W. H. & Krimm, S. (1975) *J. Appl. Phys.* **46**, 4185–4193.
16. Arnott, S., Dover, S. D. & Elliott, A. (1967) *J. Mol. Biol.* **30**, 201–208.
17. Moore, W. H. & Krimm, S. (1976) *Biopolymers* **15**, 2465–2483.
18. Krimm, S. & Abe, Y. (1972) *Proc. Natl. Acad. Sci. USA* **69**, 2788–2792.
19. Moore, W. H. & Krimm, S. (1975) *Proc. Natl. Acad. Sci. USA* **72**, 4933–4935.
20. Snyder, R. G. (1967) *J. Chem. Phys.* **47**, 1316–1360.
21. Moore, W. H. & Krimm, S. (1976) *Biopolymers* **15**, 2439–2464.
22. Krimm, S. & Dwivedi, A. M. (1972) *J. Raman Spectrosc.* **12**, 133–137.
23. Krimm, S. & Bandekar, J. (1980) *Biopolymers* **19**, 1–29.
24. Frushour, B. G. & Koenig, J. L. (1975) in *Advances in Infrared and Raman Spectroscopy*, Vol. 1, Heyden, London, pp. 35–97.
25. Hsu, S. L., Moore, W. H. & Krimm, S. (1976) *Biopolymers* **15**, 1513–1528.

Received October 28, 1983
Accepted January 2, 1984